

# IMPUTATION OF TIME-VARYING EDGE FLOWS IN GRAPHS BY MULTILINEAR KERNEL REGRESSION AND MANIFOLD LEARNING

Duc Thien Nguyen    Konstantinos Slavakis

Tokyo Institute of Technology, Japan

Department of Information and Communications Engineering  
Emails: {nguyen.t.au, slavakis.k.aa}@m.titech.ac.jp

Dimitris Pados

Florida Atlantic University, USA

Center for Connected Autonomy and Artificial Intelligence  
Department of Electrical Engineering and Computer Science  
Email: dpados@fau.edu

## ABSTRACT

This paper extends the recently developed framework of multilinear kernel regression and imputation via manifold learning (MultiL-KRIM) to impute time-varying edge flows in a graph. MultiL-KRIM uses simplicial-complex arguments and Hodge Laplacians to incorporate the graph topology, and exploits manifold-learning arguments to identify latent geometries within features which are modeled as a point-cloud around a smooth manifold embedded in a reproducing kernel Hilbert space (RKHS). Following the concept of tangent spaces to smooth manifolds, linear approximating patches are used to add a collaborative-filtering flavor to the point-cloud approximations. Together with matrix factorizations, MultiL-KRIM effects dimensionality reduction, and enables efficient computations, without any training data or additional information. Numerical tests on real-network time-varying edge flows demonstrate noticeable improvements of MultiL-KRIM over several state-of-the-art schemes.

**Index Terms**— Imputation, kernel, manifold, graph, simplicial complex.

## 1. INTRODUCTION

Graph signal processing [1–3] plays a pivotal role in modern data analytics, because signals are often associated with entities that have physical or intangible inter-connections, which are usually modeled by graphs. Due to reasons such as user privacy, sensor fault, or resources conservation, signal observation/measurement is often incomplete (missing data), causing bias and errors in subsequent stages of learning [4, 5]. Much has been done to address the missing-data problem when observed signals are associated with the nodes of a graph, e.g., [3, 6–8]. Nevertheless, many systems observe *signals over edges (edge flows)*, with the relative research gaining attention only recently [9–11].

Node-signal imputation techniques may not be successfully applied to the edge-flow imputation problem. For example, given a graph with observed signals over edges, one can consider its line-graph counterpart [12] whose nodes are edges of the original graph. In this way, the original problem is reduced to a node-signal imputation one, often solved by imposing spatial smoothness via a graph Laplacian matrix. However, this approach has been shown to produce subpar solutions as the smoothness assumption no longer holds for edge flows [13, 14]. Instead, it is more effective to assume that edge flows are almost *divergence-free*, i.e., the inbound at a node is approximately equal to the outbound, and *curl-free*, i.e., the total

flow along a “triangle” is close to zero [10, 11, 13–15]. Such assumptions are efficiently modeled by the theory of simplicial complexes and Hodge Laplacians on graphs [16]. These theories bring forth also simplicial convolutional filters, defined as matrix polynomials of Hodge Laplacians, which model the multi-hop shift of signals across simplicial complexes [17, 18].

While such theories are capable of spatial (graph topology) description, vector autoregression (VAR) is commonly used to model dependencies along time whenever edge flows are time varying [19]. However, VAR is negligent of the underlying graph topology. Recent efforts fuse simplicial convolutional filters into VAR, coined simplicial VAR (S-VAR), to take the graph topology into account, as well as to reduce the number of coefficients to be learned (dimensionality reduction) [20–22]. Notwithstanding, (S-)VAR relies by definition on past observations to predict/regress future ones, which may be problematic under the presence of missing data. Besides, VAR-based models are linear, and may thus fail to capture intricate data and feature dependencies. To address this issue, there have been studies incorporating simplicial complexes into (non-linear) neural networks [23–26], but typically, such models require large amounts of training data and intricate concatenation of non-linear layers. Further, it seems that the existing literature on simplicial-complex neural networks has not considered yet the problem of imputation of time-varying edge flows.

This paper extends the recently developed method of multilinear kernel regression and imputation via manifold learning (MultiL-KRIM) [3], and applies it to the problem of edge-flow imputation. MultiL-KRIM has been already applied to node-signal imputation [3]. Unlike (S-)VAR, where data depend directly on past observations, MultiL-KRIM assumes that missing entries can be estimated by a set of landmark points, extracted from measurements and located around a smooth manifold, embedded in an ambient reproducing kernel Hilbert space (RKHS). As such, functional approximation is enabled by the RKHS, effecting thus nonlinear data modeling, which is a lacking attribute in VAR models. Furthermore, while S-VAR applies simplicial convolutional filters for dimensionality reduction, MultiL-KRIM achieves this by matrix factorizations. Hodge Laplacians are incorporated in MultiL-KRIM’s inverse problem to take account of the graph topology. In addition, MultiL-KRIM’s manifold and tangent-space arguments model “locality,” captured in S-VAR by the number of hops in the simplicial convolutional filter. Unlike neural networks, MultiL-KRIM needs no training data and offers a more explainable approach through intuitive geometric arguments. Numerical tests on real networks show that MultiL-KRIM outperforms state-of-the-art methods.

## 2. PRELIMINARIES

A graph is denoted by  $G = (\mathcal{V}, \mathcal{E})$ , where  $\mathcal{V}$  represents the set of nodes, and  $\mathcal{E} \subseteq \mathcal{V} \times \mathcal{V}$  is the set of edges. A  $k$ -simplex  $\mathcal{S}^k \subset \mathcal{V}$

This work was supported by JST SPRING, Japan Grant Number JP-MJSP2106 and by the U.S. Air Force Office of Scientific Research, Agile Science of Test and Evaluation Program, under grants W911NF-23-S-0014 and W911NF-20-1-0283.

comprises  $k + 1$  distinct elements of  $\mathcal{V}$ . For example, a 0-simplex is a node, an 1-simplex is an edge, and a 2-simplex is a triangle. A simplicial complex (SC)  $\mathcal{X}$  is a finite collection of simplices with the inclusion property: for any simplex  $S^k \in \mathcal{X}$ , if  $S^{k-1} \subset S^k$ , then  $S^{k-1} \in \mathcal{X}$ . An SC of order  $K$ , denoted as  $\mathcal{X}^K$ , contains at least one  $K$ -simplex [10, 16].

Hodge Laplacians [16] describe adjacencies in an SC. Specifically, in an SC  $\mathcal{X}^K$ , the incidence matrix  $\mathbf{B}_k \in \mathbb{R}^{N_{k-1} \times N_k}$ ,  $k \geq 1$  captures the adjacencies between  $(k-1)$ - and  $k$ -simplices, where  $N_k$  is the number of  $k$ -simplices in  $\mathcal{X}$ . For example,  $\mathbf{B}_1$  is the node-to-edge incidence matrix and  $\mathbf{B}_2$  is the edge-to-triangle one. Incidence matrices satisfy the boundary condition  $\mathbf{B}_k \mathbf{B}_{k+1} = \mathbf{0}$ ,  $\forall k \geq 1$ . Hodge Laplacians are defined as

$$\mathbf{L}_k := \begin{cases} \mathbf{B}_{k+1} \mathbf{B}_{k+1}^\top, & \text{if } k = 0, \\ \mathbf{B}_k^\top \mathbf{B}_k + \mathbf{B}_{k+1} \mathbf{B}_{k+1}^\top, & \text{if } 1 \leq k \leq K-1, \\ \mathbf{B}_k^\top \mathbf{B}_k, & \text{if } k = K, \end{cases} \quad (1)$$

where  $\mathbf{L}_0$  is the well-known graph Laplacian matrix, which describes node-adjacencies via shared edges. Hodge Laplacian  $\mathbf{L}_1$  defines the adjacencies between edges via shared nodes by the lower-Laplacian  $\mathbf{L}_{1,l} := \mathbf{B}_1^\top \mathbf{B}_1$ , and via shared triangles by the upper-Laplacian  $\mathbf{L}_{1,u} := \mathbf{B}_2 \mathbf{B}_2^\top$ . Likewise,  $\mathbf{L}_2$  denotes the connection between triangles through common edges. As this paper concerns signals over edges,  $\mathbf{L}_1$  will be the main focus.

“Simplicial signals” are abstracted as functions which map a  $k$ -simplex to a real number. In case of time-varying signals, an “edge-flow signal” at time  $t \in \{1, 2, \dots, T\}$  is denoted by  $\mathbf{y}_t = [y_{1t}, y_{2t}, \dots, y_{N_1 t}]^\top \in \mathbb{R}^{N_1}$ . These vectors comprise the data matrix  $\mathbf{Y} = [\mathbf{y}_1, \mathbf{y}_2, \dots, \mathbf{y}_T] \in \mathbb{R}^{N_1 \times T}$ . To account for missing entries, let the index set of observed entries  $\Omega := \{(i, t) \in \{1, \dots, N_1\} \times \{1, \dots, T\} \mid y_{it} \neq +\infty\}$ , where  $+\infty$  denotes a missing entry, and define the linear *sampling mapping*  $\mathcal{S}_\Omega: (\mathbb{R} \cup \{+\infty\})^{N_1 \times T} \rightarrow \mathbb{R}^{N_1 \times T}: \mathbf{Y} \mapsto \mathcal{S}_\Omega(\mathbf{Y})$ , which operates entry-wisely as follows:  $[\mathcal{S}_\Omega(\mathbf{Y})]_{it} := [\mathbf{Y}]_{it}$ , if  $(i, t) \in \Omega$ , while  $[\mathcal{S}_\Omega(\mathbf{Y})]_{it} := 0$ , if  $(i, t) \notin \Omega$ .

An edge-flow imputation framework solves the following inverse problem

$$\begin{aligned} \min_{\mathbf{X} \in \mathbb{R}^{N_1 \times T}} \mathcal{L}(\mathbf{X}) + \mathcal{R}(\mathbf{X}) \\ \text{s.t. } \mathcal{S}_\Omega(\mathbf{Y}) = \mathcal{S}_\Omega(\mathbf{X}) \text{ and other constraints,} \end{aligned} \quad (2)$$

where  $\mathcal{L}(\cdot)$  is the data-fit loss and  $\mathcal{R}(\cdot)$  is the regularizer for structural priors, while constraint  $\mathcal{S}_\Omega(\mathbf{Y}) = \mathcal{S}_\Omega(\mathbf{X})$  preserves the consistency of the observed entries of  $\mathbf{Y}$ . For example, FlowSSL [14] sets  $\mathcal{L}(\mathbf{X}) := 0$  and  $\mathcal{R}(\mathbf{X}) := (\lambda_l/2) \|\mathbf{B}_1 \mathbf{X}\|_F^2 + (\lambda_u/2) \|\mathbf{B}_2^\top \mathbf{X}\|_F^2$ , which imposes the conservation of the flows at the nodes and cyclic flows along edges of triangles. More recent studies incorporate the Hodge Laplacians into VAR, a widely used tool for time-varying signals modeling. In particular, S-VAR [20–22] approximates each snapshot  $\mathbf{y}_t \approx \sum_{p=1}^P \mathbf{H}_p(\mathbf{L}_1) \mathbf{y}_{t-p}$ , where  $\{\mathbf{H}_p(\mathbf{L}_1)\}_{p=1}^P$  are simplicial convolutional filters [18], whose role is to capture the multi-hop dependencies between edges. As a result, S-VAR sets  $\mathcal{L}(\mathbf{X}) := \sum_{t=1}^T \|\mathbf{x}_t - \mathbf{F}_t \boldsymbol{\beta}_t\|_2^2$ , where  $\{\boldsymbol{\beta}_t\}_{t=1}^T$  are learnable parameters, and  $\{\mathbf{F}_t\}_{t=1}^T$  are “shifted signals” of  $\{\mathbf{y}_t\}_{t=1}^T$ .

### 3. PROPOSED METHOD

#### 3.1. A short recap of MultiL-KRIM

MultiL-KRIM [3] is a generic data-imputation-by-regression framework which combines matrix factorization, kernel methods and manifold learning. The approach can be shortly described as follows.

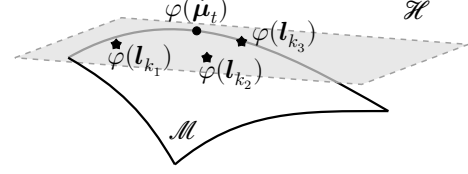


**Fig. 1:** A “collaborative-filtering” approach: Points  $\{\varphi(\mathbf{l}_{k_j})\}_{j=1}^3$ , which lie into or close to the unknown-to-the-user manifold  $\mathcal{M} \subset \mathcal{H}$ , collaborate affinely to approximate  $\varphi(\check{\boldsymbol{\mu}}_t)$ . All affine combinations of  $\{\varphi(\mathbf{l}_{k_j})\}_{j=1}^3$  define the approximating “linear patch” (gray-colored plane), which mimics the concept of a tangent space to  $\mathcal{M}$  [27].

Assuming that data  $\mathcal{S}_\Omega(\mathbf{Y})$  are faithful, a subset of  $\mathcal{S}_\Omega(\mathbf{Y})$ , called *navigator/pilot* data and denoted as  $\check{\mathbf{Y}}_f := [\check{\mathbf{y}}_1^f, \dots, \check{\mathbf{y}}_{N_{\text{nav}}}^f] \in \mathbb{R}^{\nu \times N_{\text{nav}}}$ , are selected by the user; for example, all of  $\mathcal{S}_\Omega(\mathbf{Y})$  can be selected. As the cardinality of the point-cloud  $\{\check{\mathbf{y}}_t^f\}_{t=1}^{N_{\text{nav}}}$  grows for large datasets, a subset  $\{\mathbf{l}_k\}_{k=1}^{N_l}$ , coined *landmark/representative* points, with  $N_l \leq N_{\text{nav}}$ , is selected from  $\{\check{\mathbf{y}}_t^f\}_{t=1}^{N_{\text{nav}}}$ . Several ways to form navigator data and landmark points have been suggested [3]. Let  $\check{\mathbf{L}} := [\mathbf{l}_1, \mathbf{l}_2, \dots, \mathbf{l}_{N_l}] \in \mathbb{R}^{\nu \times N_l}$ . To facilitate nonlinear approximation, a feature map  $\varphi(\cdot)$  takes vector  $\mathbf{l}_k$  to  $\varphi(\mathbf{l}_k)$  in an RKHS  $\mathcal{H}$ , equipped with a reproducing kernel  $\kappa(\cdot, \cdot): \mathbb{R}^\nu \times \mathbb{R}^\nu \rightarrow \mathbb{R}$ , with well-documented merits in approximation theory [28]. To this end,  $\varphi(\mathbf{l}) := \kappa(\mathbf{l}, \cdot) \in \mathcal{H}$ ,  $\forall \mathbf{l} \in \mathbb{R}^\nu$ . For convenience, let  $\Phi(\check{\mathbf{L}}) := [\varphi(\mathbf{l}_1), \dots, \varphi(\mathbf{l}_{N_l})]$ . Consequently,  $\mathbf{K} := \Phi(\check{\mathbf{L}})^\top \Phi(\check{\mathbf{L}})$  is an  $N_l \times N_l$  kernel matrix whose  $(k, k')$ th entry is equal to  $\langle \varphi(\mathbf{l}_k) \mid \varphi(\mathbf{l}_{k'}) \rangle_{\mathcal{H}} = \kappa(\mathbf{l}_k, \mathbf{l}_{k'})$ , where  $\top$  stands for vector/matrix transposition, and  $\langle \cdot \mid \cdot \rangle_{\mathcal{H}}$  for the inner product of the RKHS  $\mathcal{H}$ .

The flow  $x_{it}$  through the edge  $i$  at time  $t$  is approximated as

$$[\mathbf{X}]_{it} = x_{it} \approx f_i(\check{\boldsymbol{\mu}}_t) = \langle f_i \mid \varphi(\check{\boldsymbol{\mu}}_t) \rangle_{\mathcal{H}}, \quad (3)$$

where  $f_i(\cdot): \mathbb{R}^\nu \rightarrow \mathbb{R}$  is an unknown non-linear function in the RKHS functional space  $\mathcal{H}$ ,  $\check{\boldsymbol{\mu}}_t$  is an unknown vector in  $\mathbb{R}^\nu$ , and the latter part of (3) is because of the reproducing property of  $\mathcal{H}$  [28]. Motivated by the representer theorem,  $f_i$  is assumed to belong to the linear span of  $\{\varphi(\mathbf{l}_k)\}_{k=1}^{N_l}$ , i.e., there exists  $\mathbf{u}_i := [u_{i1}, \dots, u_{iN_l}]^\top \in \mathbb{R}^{N_l}$  s.t.  $f_i = \sum_{k=1}^{N_l} u_{ik} \varphi(\mathbf{l}_k) = \Phi(\check{\mathbf{L}}) \mathbf{u}_i$ . Regarding  $\varphi(\check{\boldsymbol{\mu}}_t)$ , the concept of tangent spaces to smooth manifolds [27] offers also a “collaborative-filtering” flavor to the design: it is assumed that  $\varphi(\check{\boldsymbol{\mu}}_t)$  lies into or close to  $\mathcal{M}$  and is approximated by only a few members of  $\{\varphi(\mathbf{l}_k)\}_{k=1}^{N_l}$  which collaborate *affinely*, i.e., there exists a sparse vector  $\mathbf{v}_t \in \mathbb{R}^{N_l}$  s.t.  $\varphi(\check{\boldsymbol{\mu}}_t) = \Phi(\check{\mathbf{L}}) \mathbf{v}_t$ , under the affine constraint  $\mathbf{1}_{N_l}^\top \mathbf{v}_t = 1$ , where  $\mathbf{1}_{N_l}$  is the  $N_l \times 1$  all-one vector; cf., Figure 1.

So far, the entry-wise estimation  $[\mathbf{X}]_{it} \approx f_i(\check{\boldsymbol{\mu}}_t) = \langle f_i \mid \varphi(\check{\boldsymbol{\mu}}_t) \rangle_{\mathcal{H}} = \langle \Phi(\check{\mathbf{L}}) \mathbf{u}_i \mid \Phi(\check{\mathbf{L}}) \mathbf{v}_t \rangle_{\mathcal{H}} = \mathbf{u}_i^\top \mathbf{K} \mathbf{v}_t$ . To offer compact notations, if  $\mathbf{U} := [\mathbf{u}_1, \dots, \mathbf{u}_{N_l}]^\top \in \mathbb{R}^{N_l \times N_l}$  and  $\mathbf{V} := [\mathbf{v}_1, \dots, \mathbf{v}_T] \in \mathbb{R}^{N_l \times T}$ , then data are modeled as

$$\mathbf{X} \approx \mathbf{U} \mathbf{K} \mathbf{V}, \quad (4)$$

where  $\mathbf{V}$  is a sparse matrix satisfying  $\mathbf{1}_{N_l}^\top \mathbf{V} = \mathbf{1}_T^\top$ . To ease the excessive cost caused by large  $N_l$  and  $N_l$ , [3] employs multilinear factorization  $\mathbf{U} = \mathbf{U}_1 \mathbf{U}_2 \dots \mathbf{U}_Q$ , which has been shown to be highly efficient, especially for high-dimensional dynamic imaging data [3].

#### 3.2. Extended MultiL-KRIM for edge-flow imputation

In large networks with long time series, sizes  $N_1, T$ , and  $N_l$  can cause massive burden. Unlike S-VAR [20–22], which reduces the model size of VAR by simplicial convolutional filters, and [3], which

factors only  $\mathbf{U}$  in (4), this paper suggests the following factorization

$$\mathbf{X} \approx \mathbf{U}_1 \mathbf{U}_2 \mathbf{K} \mathbf{V}_1 \mathbf{V}_2, \quad (5)$$

where the inner matrix dimensions  $d, r \ll N_l$  are user-defined. Based on findings in [3], factorizing  $\mathbf{U}$  further, by more than two factors, does not notably improve the accuracy, so  $\mathbf{U} = \mathbf{U}_1 \mathbf{U}_2$  and  $\mathbf{V} = \mathbf{V}_1 \mathbf{V}_2$  are used here. It can be easily checked that the affine constraint of  $\mathbf{V}$  in (4) still holds after enforcing  $\mathbf{1}_{N_l}^\top \mathbf{V}_1 = \mathbf{1}_r^\top$  and  $\mathbf{1}_r^\top \mathbf{V}_2 = \mathbf{1}_T^\top$ .

Ultimately, following the common assumption that edge flows are approximately *divergence-free* and *curl-free* (cf., Section 2), the extended MultiL-KRIM inverse problem for edge-flow imputation is formed as

$$\min_{(\mathbf{x}, \mathbf{U}_1, \mathbf{U}_2, \mathbf{V}_1, \mathbf{V}_2)} \frac{1}{2} \|\mathbf{X} - \mathbf{U}_1 \mathbf{U}_2 \mathbf{K} \mathbf{V}_1 \mathbf{V}_2\|_F^2 + \frac{\lambda_l}{2} \|\mathbf{B}_1 \mathbf{X}\|_F^2 + \frac{\lambda_u}{2} \|\mathbf{B}_2^\top \mathbf{X}\|_F^2 \quad (6a)$$

$$+ \frac{\lambda_2}{2} \sum_{q=1}^2 \|\mathbf{U}_q\|_F^2 + \lambda_1 \sum_{p=1}^2 \|\mathbf{V}_p\|_1 \quad (6a)$$

$$\text{s.to } \mathcal{S}_\Omega(\mathbf{Y}) = \mathcal{S}_\Omega(\mathbf{X}), \quad (6b)$$

$$\mathbf{1}_{N_l}^\top \mathbf{V}_1 = \mathbf{1}_r^\top, \quad (6c)$$

$$\mathbf{1}_r^\top \mathbf{V}_2 = \mathbf{1}_T^\top.$$

The loss function is non-convex, and to guarantee convergence to a critical point, the parallel successive-convex-approximation (SCA) framework of [29] is utilized. The algorithm is summarized in Algorithm 1, where the following tuple of estimates  $\forall n \in \mathbb{N}, \forall k \in \{0, 1\}$ ,

$$\hat{\mathcal{O}}^{(n+k/2)} := (\hat{\mathbf{X}}^{(n+k/2)}, \hat{\mathbf{U}}_1^{(n+k/2)}, \hat{\mathbf{U}}_2^{(n+k/2)}, \hat{\mathbf{V}}_1^{(n+k/2)}, \hat{\mathbf{V}}_2^{(n+k/2)}), \quad (7)$$

is recursively updated via the following convex sub-tasks which can be solved in parallel at every iteration  $n$ :

$$\hat{\mathbf{X}}^{(n+1/2)} := \arg \min_{\mathbf{X}} \frac{1}{2} \|\mathbf{X} - \hat{\mathbf{U}}_1^{(n)} \hat{\mathbf{U}}_2^{(n)} \mathbf{K} \hat{\mathbf{V}}_1^{(n)} \hat{\mathbf{V}}_2^{(n)}\|_F^2 + \frac{\lambda_l}{2} \|\mathbf{B}_1 \mathbf{X}\|_F^2 + \frac{\lambda_u}{2} \|\mathbf{B}_2^\top \mathbf{X}\|_F^2 + \frac{\tau_X}{2} \|\mathbf{X} - \hat{\mathbf{X}}^{(n)}\|_F^2 \quad (8a)$$

$$\text{s.to } \mathcal{S}_\Omega(\mathbf{Y}) = \mathcal{S}_\Omega(\mathbf{X}),$$

$$\hat{\mathbf{U}}_1^{(n+1/2)} := \arg \min_{\mathbf{U}_1} \frac{1}{2} \|\hat{\mathbf{X}}^{(n)} - \mathbf{U}_1 \hat{\mathbf{U}}_2^{(n)} \mathbf{K} \hat{\mathbf{V}}_1^{(n)} \hat{\mathbf{V}}_2^{(n)}\|_F^2 + \frac{\lambda_2}{2} \|\mathbf{U}_1\|_F^2 + \frac{\tau_U}{2} \|\mathbf{U}_1 - \hat{\mathbf{U}}_1^{(n)}\|_F^2, \quad (8b)$$

$$\hat{\mathbf{U}}_2^{(n+1/2)} := \arg \min_{\mathbf{U}_2} \frac{1}{2} \|\hat{\mathbf{X}}^{(n)} - \hat{\mathbf{U}}_1^{(n)} \mathbf{U}_2 \mathbf{K} \hat{\mathbf{V}}_1^{(n)} \hat{\mathbf{V}}_2^{(n)}\|_F^2 + \frac{\lambda_2}{2} \|\mathbf{U}_2\|_F^2 + \frac{\tau_U}{2} \|\mathbf{U}_2 - \hat{\mathbf{U}}_2^{(n)}\|_F^2, \quad (8c)$$

$$\hat{\mathbf{V}}_1^{(n+1/2)} := \arg \min_{\mathbf{V}_1} \frac{1}{2} \|\hat{\mathbf{X}}^{(n)} - \hat{\mathbf{U}}_1^{(n)} \hat{\mathbf{U}}_2^{(n)} \mathbf{K} \mathbf{V}_1 \hat{\mathbf{V}}_2^{(n)}\|_F^2 + \lambda_1 \|\mathbf{V}_1\|_1 + \frac{\tau_V}{2} \|\mathbf{V}_1 - \hat{\mathbf{V}}_1^{(n)}\|_F^2 \quad (8d)$$

$$\text{s.to } \mathbf{1}_{N_l}^\top \mathbf{V}_1 = \mathbf{1}_r^\top,$$

---

### Algorithm 1 Solving MultiL-KRIM's inverse problem

---

**Input:**

**Output:** Limit point  $\hat{\mathcal{O}}^{(*)}$  of sequence  $(\hat{\mathcal{O}}^{(n)})_{n \in \mathbb{N}}$ .

- 1: Fix  $\hat{\mathcal{O}}^{(0)}$ ,  $\gamma_0 \in (0, 1]$ , and  $\zeta \in (0, 1)$ .
  - 2: **while**  $n \geq 0$  **do**
  - 3: Available are  $\hat{\mathcal{O}}^{(n)}$  (7).
  - 4:  $\gamma_{n+1} := \gamma_n(1 - \zeta\gamma_n)$ .
  - 5: Solve in parallel the convex sub-tasks (8).
  - 6:  $\hat{\mathcal{O}}^{(n+1)} := \gamma_{n+1} \hat{\mathcal{O}}^{(n+1/2)} + (1 - \gamma_{n+1}) \hat{\mathcal{O}}^{(n)}$ .
  - 7: Set  $n \leftarrow n + 1$  and go to step 2.
  - 8: **end while**
- 

$$\hat{\mathbf{V}}_2^{(n+1/2)} := \arg \min_{\mathbf{V}_2} \frac{1}{2} \|\hat{\mathbf{X}}^{(n)} - \hat{\mathbf{U}}_1^{(n)} \hat{\mathbf{U}}_2^{(n)} \mathbf{K} \mathbf{V}_1^{(n)} \mathbf{V}_2\|_F^2 + \lambda_1 \|\mathbf{V}_2\|_1 + \frac{\tau_V}{2} \|\mathbf{V}_2 - \hat{\mathbf{V}}_2^{(n)}\|_F^2 \quad (8e)$$

$$\text{s.to } \mathbf{1}_r^\top \mathbf{V}_2 = \mathbf{1}_T^\top,$$

where the user-defined  $\tau_X, \tau_U, \tau_V, \lambda_1, \lambda_2, \lambda_l, \lambda_u \in \mathbb{R}_{++}$ . Sub-tasks (8d) and (8e) are composite convex minimization tasks under affine constraints, and can be thus solved iteratively by [30], while (8a), (8b), and (8c) have closed-form solutions.

### 3.3. Computational complexity

The number of unknown parameters in (5) is  $(N_1 + N_l)d + (N_l + T)r$ . Per iteration  $n$  in Algorithm 1, the computational complexity of sub-task (8b) is  $\mathcal{O}(N_1 d^2 + d^3)$ , and that of (8c) is  $\mathcal{O}(d^3 + N_l^3)$ . Meanwhile, the complexity of sub-task (8d) is  $\mathcal{O}(K_1 N_l^2 d)$ , and that of (8e) is  $\mathcal{O}(K_2 d^2 T)$ , where  $K_1$  and  $K_2$  are the numbers of iterations that [30] takes to solve (8d) and (8e), respectively.

## 4. NUMERICAL TESTS

MultiL-KRIM is tested on the traffic flows in Sioux Falls transportation network [31] and on the water flows in the Cherry Hills water network [32]. MultiL-KRIM is compared against the state-of-the-art edge-flow imputation methods FlowSSL [14] and S-VAR [20–22]. As a baseline for matrix-factorization techniques, the multi-layer matrix factorization (MMF) [33] is implemented. Here, MMF [33] solves the same inverse problem (6) as MultiL-KRIM, but with the kernel matrix  $\mathbf{K} = \mathbf{I}_{N_l}$  in (5). In other words, MMF [33] is a *blind* matrix-factorization method, where no data geometry/patterns are explored and exploited, as in Figure 1, and no functional approximation via RKHSs is employed.

The evaluation metric is the mean absolute error (MAE) (lower is better), defined as  $\text{MAE} := \|\mathbf{X} - \mathbf{Y}\|_1 / (N_1 \cdot T)$ , where  $\mathbf{Y}$  is the fully-sampled data,  $\mathbf{X}$  gathers all reconstructed flows, and  $\|\cdot\|_1$  is the  $\ell_1$ -norm. All methods are finely tuned to achieve their lowest MAE. Reported metric values are mean values of 30 independent runs. Source codes of FlowSSL [14] and S-VAR [20–22] were made publicly available by the authors. Source code for MultiL-KRIM and MMF was written in Julia [34]. All tests were run on an 8-core Intel(R) i7-11700 2.50GHz CPU with 32GB RAM.

With sampling ratio  $s \in \{0.1, 0.2, 0.3, 0.4, 0.5\}$ , signals of  $\lceil N_1 \cdot s \rceil$  edges are sampled per time instant  $t$ , where  $\lceil \cdot \rceil$  is the ceiling function. This sampling pattern suggests that the number of observations is consistent along time. Navigator data  $\hat{\mathbf{Y}}_{\text{nav}}$  are formed by the snapshots, that is, columns of  $\mathcal{S}_\Omega(\mathbf{Y})$  after removing all the unobserved entries. Landmark points are selected by the greedy max-min-distance strategy [35], based on Euclidean distances among navigator data. Hyperparameters  $\tau_X = \tau_U = \tau_V = 2$  in (8) to ensure

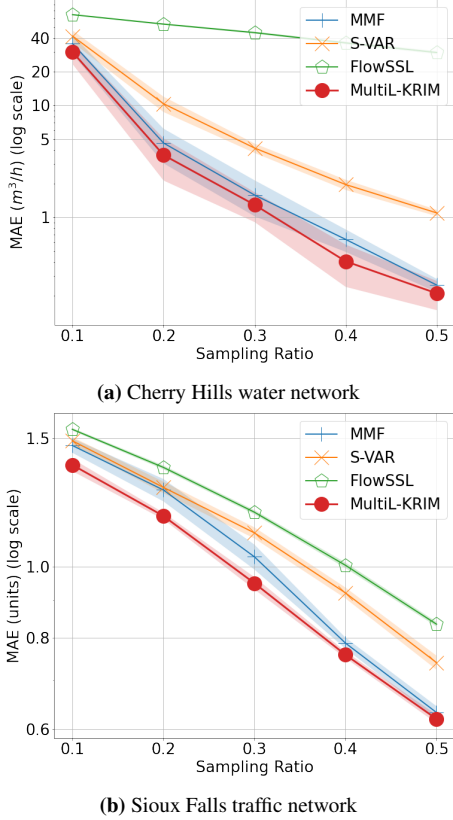


**Fig. 2:** Mean MAE value curves in log scale (the lower the better) w.r.t. the ground truth signals vs. sampling ratios. The shaded areas indicate a range of one standard deviation above and below the mean.

Datasets \ Methods	S-VAR	MMF	MultiL-KRIM
Cherry Hills	30,000	6,400	6,400
Sioux Falls	15,000	2,190	2,190

**Table 1:** Number of unknown parameters.

stability of the algorithm. Meanwhile, regularization hyperparameters  $\lambda_1, \lambda_2, \lambda_l$ , and  $\lambda_u$  in (8), the number of landmark points  $N_l$ , and inner dimensions  $d, r$  in (5) are identified by grid-search.

#### 4.1. Cherry Hills water network

Cherry Hills water network consists of 36 nodes (0-simplices), 40 pipes (1-simplices), and 2 triangles (2-simplices) [32]. Time-varying water flow over the network is generated using the EPANET software [36]. Flows are measured hourly in cubic meter per hour ( $\text{m}^3/\text{h}$ ) in a span of 300 hours. The size of data  $\mathbf{Y}$  is  $40 \times 300$ , and the number of landmark points is  $N_l = 150$ . Figure 2a shows MAE values of competing methods across different sampling ratios. MultiL-KRIM outperforms the competing methods at every sampling ratio. It significantly outperforms S-VAR [20–22], especially at higher sampling ratios. FlowSSL [14], which solely depends on the Hodge Laplacians-based regularizers, scores much higher MAE values than the other methods. MultiL-KRIM outperforms also the blind matrix-factorization MMF [33].

Figure 3 visualizes the coefficient matrices learned by Algorithm 1. In particular, Figures 3c and 3d draw the heatmaps of  $\hat{\mathbf{V}}_1^{(*)}$  and  $\hat{\mathbf{V}}_2^{(*)}$  of Algorithm 1, respectively. The heatmaps show that  $\hat{\mathbf{V}}_2^{(*)}$  and especially  $\hat{\mathbf{V}}_1^{(*)}$  are sparse. The portion of entries whose abso-

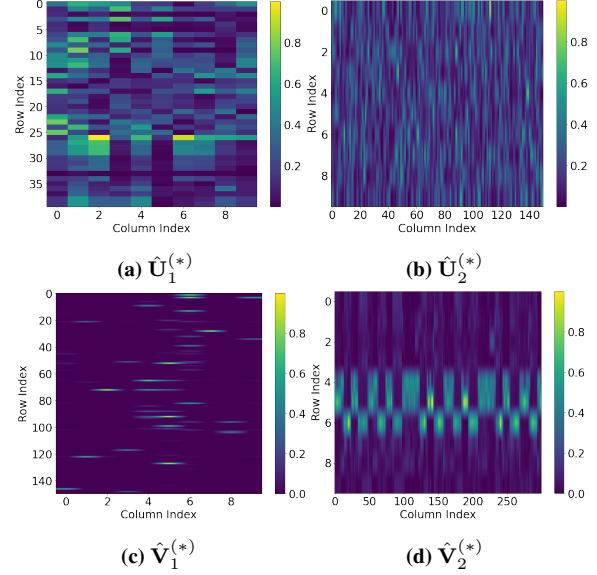


**Fig. 3:** Visualization of coefficient matrices  $\hat{\mathbf{U}}_1^{(*)}, \hat{\mathbf{U}}_2^{(*)}, \hat{\mathbf{V}}_1^{(*)}$  and  $\hat{\mathbf{V}}_2^{(*)}$ , output by Algorithm 1 for Cherry Hills water network data, at sampling ratio  $s = 0.5$ . Heat maps show the entry-wise absolute values of the matrices, rescaled to be in  $[0, 1]$  range.

lute value is larger than 0.001 is 9.1% in  $\hat{\mathbf{V}}_1^{(*)}$  and 89.6% in  $\hat{\mathbf{V}}_2^{(*)}$ . In contrast, by Figures 3a and 3b,  $\hat{\mathbf{U}}_1^{(*)}, \hat{\mathbf{U}}_2^{(*)}$  are dense, where the percentage of entries whose absolute value is larger than 0.001 is 98.8% in  $\hat{\mathbf{U}}_1^{(*)}$  and 99.8% in  $\hat{\mathbf{U}}_2^{(*)}$ .

#### 4.2. Sioux Falls transportation network

The Sioux Falls transportation network has 24 nodes (0-simplices), 38 edges (1-simplices), and 2 triangles (2-simplices) [31]. The synthetic time-varying traffic flow is generated as in [20, 22], so that it contains both divergence flows and cyclic flows. The measurement unit is neglected, simply denoted as “units.” The size of data  $\mathbf{Y}$  is  $38 \times 300$ , while  $N_l = 50$ . Figure 2b plots MAE curves against sampling ratios. MultiL-KRIM continues to outperform the competing methods, with notable gaps when compared with S-VAR [20–22] and FlowSSL [14]. Meanwhile, the gap between MultiL-KRIM and MMF [33] accentuates at lower sampling ratios. FlowSSL [14] scores again the highest MAE values.

With regards to dimensionality reduction, Table 1 compares the number of unknown parameters in S-VAR [20–22], MMF [33], and MultiL-KRIM. Although the number of parameters of MultiL-KRIM are 21.3% (Cherry Hills) and 14.6% (Sioux Falls) of those of S-VAR, MultiL-KRIM still outperforms in both datasets.

## 5. CONCLUSIONS

This paper applied the recently developed MultiL-KRIM, a multilinear kernel-regression-imputation and manifold-learning framework, into the time-varying edge-flow imputation problem. MultiL-KRIM approximated data via simple geometric arguments and facilitated computation by low-rank matrix factorization, without the need for training data. To further realize the common priors of edge flows, MultiL-KRIM’s inverse problem incorporated also the graph’s Hodge Laplacians. Numerical tests on real water and traffic networks showed that MultiL-KRIM offers better performance than several state-of-the-art methods.

## REFERENCES

- [1] A. Ortega, P. Frossard, J. Kovačević, J. M. Moura, and P. Vandergheynst, "Graph signal processing: Overview, challenges, and applications," *Proceedings of the IEEE*, vol. 106, no. 5, pp. 808–828, 2018.
- [2] G. Leus, A. G. Marques, J. M. Moura, A. Ortega, and D. I. Shuman, "Graph signal processing: History, development, impact, and outlook," *IEEE Signal Processing Magazine*, vol. 40, no. 4, pp. 49–60, 2023.
- [3] D. T. Nguyen and K. Slavakis, "Multilinear kernel regression and imputation via manifold learning," *IEEE Open Journal of Signal Processing*, pp. 1–15, 2024. DOI: 10.1109/OJSP.2024.3444707.
- [4] S. Chen, A. Sandryhaila, J. M. Moura, and J. Kovačević, "Signal recovery on graphs: Variation minimization," *IEEE Trans. Signal Processing*, vol. 63, no. 17, pp. 4609–4624, 2015.
- [5] S. Chen, R. Varma, A. Singh, and J. Kovačević, "Signal recovery on graphs: Fundamental limits of sampling strategies," *IEEE Transactions on Signal and Information Processing over Networks*, vol. 2, no. 4, pp. 539–554, 2016.
- [6] K. Qiu, X. Mao, X. Shen, X. Wang, T. Li, and Y. Gu, "Time-varying graph signal reconstruction," *IEEE Journal of Selected Topics in Signal Processing*, vol. 11, no. 6, pp. 870–883, 2017.
- [7] D. Romero, V. N. Ioannidis, and G. B. Giannakis, "Kernel-based reconstruction of space-time functions on dynamic graphs," *IEEE Journal of Selected Topics in Signal Processing*, vol. 11, no. 6, pp. 856–869, 2017.
- [8] J. A. Castro-Correa, J. H. Giraldo, M. Badiey, and F. D. Malliaros, "Gegenbauer graph neural networks for time-varying signal reconstruction," *IEEE Transactions on Neural Networks and Learning Systems*, pp. 1–, 2024. DOI: 10.1109/TNNLS.2024.3381069.
- [9] F. Battiston, G. Cencetti, I. Iacopini, V. Latora, M. Lucas, A. Patania, J.-G. Young, and G. Petri, "Networks beyond pairwise interactions: Structure and dynamics," *Physics Reports*, vol. 874, pp. 1–92, 2020.
- [10] S. Barbarossa and S. Sardellitti, "Topological signal processing over simplicial complexes," *IEEE Trans. Signal Processing*, vol. 68, pp. 2992–3007, 2020.
- [11] M. T. Schaub, Y. Zhu, J.-B. Seby, T. M. Roddenberry, and S. Segarra, "Signal processing on higher-order networks: Livin' on the edge... and beyond," *Signal Processing*, vol. 187, p. 108 149, 2021.
- [12] T. S. Evans and R. Lambiotte, "Line graphs, link partitions, and overlapping communities," *Physical Review E—Statistical, Nonlinear, and Soft Matter Physics*, vol. 80, no. 1, p. 016 105, 2009.
- [13] M. T. Schaub and S. Segarra, "Flow smoothing and denoising: Graph signal processing in the edge-space," in *IEEE Global Conference on Signal and Information Processing (GlobalSIP)*, 2018, pp. 735–739.
- [14] J. Jia, M. T. Schaub, S. Segarra, and A. R. Benson, "Graph-based semi-supervised & active learning for edge flows," in *SIGKDD International Conference on Knowledge Discovery & Data Mining*, 2019, pp. 761–771.
- [15] M. Yang and E. Isufi, "Simplicial trend filtering," in *2022 56th Asilomar Conference on Signals, Systems, and Computers*, IEEE, 2022, pp. 930–934.
- [16] L.-H. Lim, "Hodge Laplacians on graphs," *SIAM Review*, vol. 62, no. 3, pp. 685–715, 2020.
- [17] E. Isufi and M. Yang, "Convolutional filtering in simplicial complexes," in *IEEE International Conference on Acoustics, Speech and Signal Processing (ICASSP)*, 2022, pp. 5578–5582.
- [18] M. Yang, E. Isufi, M. T. Schaub, and G. Leus, "Simplicial convolutional filters," *IEEE Trans. Signal Processing*, vol. 70, pp. 4633–4648, 2022.
- [19] R. Money, J. Krishnan, B. Beferull-Lozano, and E. Isufi, "Online edge flow imputation on networks," *IEEE Signal Processing Letters*, vol. 30, pp. 115–119, 2022.
- [20] J. Krishnan, R. Money, B. Beferull-Lozano, and E. Isufi, "Simplicial vector autoregressive model for streaming edge flows," in *IEEE International Conference on Acoustics, Speech and Signal Processing (ICASSP)*, 2023, pp. 1–5.
- [21] J. Krishnan, R. Money, B. Beferull-Lozano, and E. Isufi, "Simplicial vector autoregressive models," *Authorea Preprints*, 2024.
- [22] R. Money, J. Krishnan, B. Beferull-Lozano, and E. Isufi, "Evolution backcasting of edge flows from partial observations using simplicial vector autoregressive models," in *IEEE International Conference on Acoustics, Speech and Signal Processing (ICASSP)*, 2024, pp. 9516–9520.
- [23] S. Ebli, M. Defferrard, and G. Spreemann, "Simplicial neural networks," in *TDA & Beyond*, 2020.
- [24] T. M. Roddenberry, N. Glaze, and S. Segarra, "Principled simplicial neural networks for trajectory prediction," in *International Conference on Machine Learning*, PMLR, 2021, pp. 9020–9029.
- [25] M. Yang, E. Isufi, and G. Leus, "Simplicial convolutional neural networks," in *IEEE International Conference on Acoustics, Speech and Signal Processing (ICASSP)*, 2022, pp. 8847–8851.
- [26] H. Wu, A. Yip, J. Long, J. Zhang, and M. K. Ng, "Simplicial complex neural networks," *IEEE Transactions on Pattern Analysis and Machine Intelligence*, vol. 46, no. 1, pp. 561–575, 2024. DOI: 10.1109/TPAMI.2023.3323624.
- [27] J. W. Robbin and D. A. Salamon, *Introduction to Differential Geometry*. Berlin: Springer, 2022.
- [28] N. Aronszajn, "Theory of reproducing kernels," *Trans. American Mathematical Society*, vol. 68, no. 3, pp. 337–404, 1950.
- [29] F. Facchinei, G. Scutari, and S. Sagratella, "Parallel selective algorithms for nonconvex big data optimization," *IEEE Trans. Signal Processing*, vol. 63, no. 7, pp. 1874–1889, 2015.
- [30] K. Slavakis and I. Yamada, "Fejér-monotone hybrid steepest descent method for finely constrained and composite convex minimization tasks," *Optimization*, vol. 67, no. 11, pp. 1963–2001, 2018.
- [31] L. A. Rossman, R. M. Clark, and W. M. Grayman, "Modeling chlorine residuals in drinking-water distribution systems," *Journal of Environmental Engineering*, vol. 120, no. 4, pp. 803–820, 1994.
- [32] L. J. Leblanc, "An algorithm for the discrete network design problem," *Transportation Science*, vol. 9, no. 3, pp. 183–199, 1975.
- [33] A. Cichocki and R. Zdunek, "Multilayer nonnegative matrix factorization using projected gradient approaches," *International Journal of Neural Systems*, vol. 17, no. 06, pp. 431–446, 2007.
- [34] J. Bezanson, A. Edelman, S. Karpinski, and V. B. Shah, "Julia: A fresh approach to numerical computing," *SIAM Review*, vol. 59, no. 1, pp. 65–98, 2017.
- [35] V. De Silva and J. B. Tenenbaum, "Sparse multidimensional scaling using landmark points," Stanford University, Tech. Rep., 2004.
- [36] L. A. Rossman, "An overview of epanet version 3.0," *Water Distribution Systems Analysis*, pp. 14–18, 2010.